



Evaluation and projection of daily maximum and minimum temperatures over China using the high-resolution NEX-GDDP dataset

Yi Wu¹ · Chiyuan Miao¹ · Qingyun Duan¹ · Chenwei Shen¹ · Xuewei Fan¹

Received: 27 January 2020 / Accepted: 29 July 2020 / Published online: 6 August 2020
© Springer-Verlag GmbH Germany, part of Springer Nature 2020

Abstract

A new bias-corrected, statistically downscaled product, the NASA Earth Exchange Global Daily Downscaled Projections (NEX-GDDP) dataset, has been developed and released to help in understanding climate change at local to regional scales. Here, we evaluate the performance of the NEX-GDDP data in simulating daily maximum temperature (TX) and daily minimum temperature (TN) in the historical period 1961–2005 over China at national and regional scales. Projected future changes in TX and TN are assessed under the Representative Concentration Pathways (RCPs) 4.5 and 8.5 emissions scenarios. Results show that the NEX-GDDP data can capture the basic spatial patterns of TX and TN, but these results underestimate the warming trends of TX and TN from 1961 to 2005 over China. The largest biases are found in western China due to its complex terrain conditions; these biases are 2.33 and 2.21 times larger than those found in eastern China for TX and TN, respectively. The climate projections show that the difference in uncertainties is small between the east and the west, and higher warming changes correspond to greater uncertainties. The increasing trends under the RCP8.5 are 2.22 and 2.31 times the size found under the RCP4.5 by the end of the twenty-first century for TX and TN, respectively. The Tibetan plateau has the fastest warming trend under the two scenarios.

Keywords Daily maximum temperature · Daily minimum temperature · NEX-GDDP data · China

1 Introduction

The phenomenon of global warming has generated great concern worldwide, because it has a series of effects on the natural environment and human society (Smith et al. 2015; Matthews et al. 2017; Sun et al. 2019; Gou et al. 2020; Sun et al. 2020). In recent years, some extreme climate events such as floods (Blöschl et al. 2017), droughts (Mazdiyasni and AghaKouchak 2015) have had great impacts on humans and ecosystems. Among them, the influence of extreme maximum and minimum temperature events is most widespread and obvious, and observations show that the frequency of these events is increasing (Yin et al. 2015;

Zheng et al. 2019). The fifth assessment report of the Intergovernmental Panel on Climate Change (IPCC) points out that future global temperature will continue to increase and the occurrence of extreme weather and climate events will become more frequent (IPCC 2014). To face future climate change with better information and reduce the economic losses caused by extreme maximum and minimum temperatures, increasingly sophisticated climate models have been developed over time. Today, most research on climate change relies on global climate models (IPCC 2014). As an important means to simulate and predict climate change of the past and future, global climate models (GCMs) have been widely used in various research fields, such as agriculture (Dawson et al. 2014), hydrology (Gosling and Arnell 2013) and so on. The fifth phase of the Coupled Model Intercomparison Project (CMIP5) has provided data that supports related research in various fields at regional and local scales (Taylor et al. 2012).

Most GCMs run on grids of relatively coarse resolution, which limits their ability to capture the spatial details of regions. The spatial resolution of most CMIP5 models is relatively low, and it varies from model to model. Therefore,

Electronic supplementary material The online version of this article (<https://doi.org/10.1007/s00382-020-05404-1>) contains supplementary material, which is available to authorized users.

✉ Chiyuan Miao
miaocy@vip.sina.com

¹ State Key Laboratory of Earth Surface Processes and Resource Ecology, Faculty of Geographical Science, Beijing Normal University, Beijing 100875, China

when using CMIP5 data, an interpolation method is usually used to unify the data to the same resolution (Jiang et al. 2016); however, this alone still cannot meet the needs of regional climate change research. Over the past decade, a variety of dynamical and statistical downscaling methods have been widely used in the field of climate change (Liu et al. 2012; Sunyer et al. 2012). In June 2015, a high-resolution NASA Earth Exchange Global Daily Downscaled Projections (NEX-GDDP) dataset was released. The NEX-GDDP dataset is produced using results from downscaled climate models under two of the four greenhouse gas emissions scenarios known as Representative Concentration Pathways (RCPs) (Meinshausen et al. 2011), which are derived from the GCM runs conducted under CMIP5 (Taylor et al. 2012). The dataset was provided to promote scientific research at regional scales and enhance public understanding about future climate change (Thrasher et al. 2013). Generating the NEX-GDDP dataset requires two steps. First, biases of the CMIP5 model data are corrected by comparing with observation data; then, high-resolution model data is obtained through a statistical downscaling method—the bias-correction spatial disaggregation (BCSD) method. The BCSD method that is used to generate the NEX-GDDP dataset is specifically designed to address some limitations of current GCMs' outputs (Wood et al. 2002, 2004; Maurer and Hidalgo 2008; Thrasher et al. 2012). The resulting dataset contains daily precipitation, daily maximum temperature and daily minimum temperature data of 21 CMIP5 models, and it has a spatial resolution of $0.25^\circ \times 0.25^\circ$ resulting from the statistical downscaling method (Taylor et al. 2012). Compared with raw CMIP5 model data, NEX-GDDP can provide more detailed information at regional scales on climate change, and the biases of model simulation results are greatly reduced (Bao and Wen 2017).

Many researchers have used the NEX-GDDP data to conduct research in various regions worldwide. Projections for future heat waves over Pakistan were analyzed using NEX-GDDP, and results indicate an increase in the number of both heat wave events and heat wave days in Pakistan (Ali et al. 2018). Thilakarathne and Sridhar (2017) studied characterization of future drought conditions in the Lower Mekong River Basin using NEX-GDDP, and report that the area is expected to experience more severe and intense droughts. Nauman et al. (2019) assessed the impact of future climate change on streamflows upstream of Khanpur Dam in Pakistan using NEX-GDDP, and the study indicates that the maximum and minimum temperatures are anticipated to increase from RCP4.5 to RCP8.5 in the future. In a study evaluating over Southeast Asia, the warming trend was overestimated compared with Climate Research Unit (CRU) observations (Raghavan et al. 2018). A study investigating the advantages of using NEX-GDDP over CMIP5 and data from the Coordinated Regional Climate Downscaling Experiment

(CORDEX) for simulating the Indian summer monsoon was also conducted, and it was found that NEX-GDDP can capture the relevant spatial patterns of seasonal mean temperatures and precipitation with the highest accuracy and fewest errors (Jain et al. 2019). The centennial drought outlook over the contiguous United States was investigated using the NASA-NEX downscaled climate ensemble, and researchers found a tendency toward more frequent and intense summer droughts (Ahmadalipour et al. 2017). Furthermore, studies on rice exposure to heat stress (Zhang et al. 2018a, b) and malaria hotspots (Semakula et al. 2017) were also conducted using NEX-GDDP. However, research using NEX-GDDP over China is relatively rare. Currently, only a few such studies have been conducted, focusing on drought (Cao and Gao 2019), extreme precipitation (Chen et al. 2017), population exposure to extreme heat (Huang et al. 2018) and so on. Other relevant research over China has focused only on small watersheds or regions (Zhang et al. 2018a, b). In general, most research over China as a whole has focused on extreme climate events, and few studies have paid close attention to temperature extremes. Small-scale studies are often conducted, while research over China as a whole is relatively scarce. At the same time, China is one of the regions with the largest climate variability in the world due to its unique geographical location and monsoon climate (Zhou and Yu 2006). Research conducted over China as a whole requires high-resolution data due to its complex terrain, and high-resolution data can better show the detailed characteristics of climate change over China (Gao et al. 2012; Guo and Wang 2016). Therefore, in light of past global warming and the continuing warming expected in the future, the study of daily maximum and minimum temperatures using NEX-GDDP over China has become an urgent task for climate change research.

2 Data and methods

2.1 Data

The observed daily maximum temperature (TX) and daily minimum temperature (TN) in mainland China during the period 1961–2005 were obtained from the China surface temperature $0.5^\circ \times 0.5^\circ$ gridded dataset (V2.0), developed by the National Meteorological Information Center, China Meteorological Administration. The datasets are constructed from 2472 station observations (Fig. 1).

Modeled TX and TN from NEX-GDDP were used in this study (data available at <https://cds.nccs.nasa.gov/nex-gddp>). Results from 21 models (Table S1) for historical simulations (1961–2005) and future projections (2006–2099) under a medium-emissions scenario (RCP4.5) and a high-emissions scenario (RCP8.5) were involved in this study. We defined

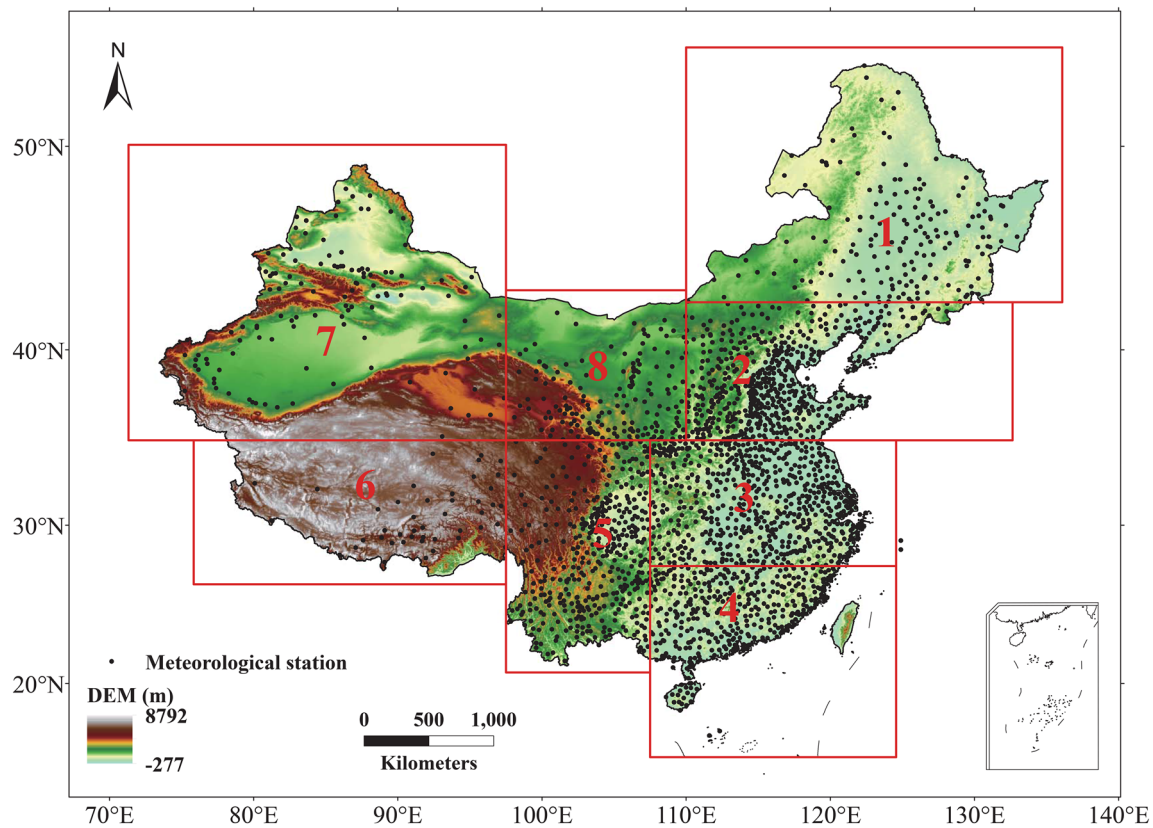


Fig. 1 The regional divisions over China (subregion 1: Northeast China (NEC), subregion 2: North China (NC), subregion 3: Jianghuai (JH), subregion 4: South China (SC), subregion 5: Southwest China

(SWC), subregion 6: Tibetan plateau (TP), subregion 7: Western part of Northwest China (WNW), subregion 8: Eastern part of Northwest China (ENW))

a 30-year baseline period for our analyses as 1970–1999. The raw resolution of NEX-GDDP data is $0.25^\circ \times 0.25^\circ$, and for evaluative purposes, all NEX-GDDP outputs in historical simulations were upscaled to the same resolution as the observed data ($0.5^\circ \times 0.5^\circ$ grid) by averaging every 2×2 pixels.

2.2 Methodology

In the following analyses, we evaluate the performance of NEX-GDDP model outputs during the historical period (1961–2005) and then project future scenarios over the medium-term (2040–2069) and long-term (2070–2099) future periods. There are many uncertainties in the evaluation of climate change, and multi-model ensembles (MMEs) are considered to be effective in reducing the uncertainties (Dale et al. 2017). MME estimation results are also more reliable than estimations from single models (Slater et al. 2016). Therefore, an MME was constructed by applying equal weights to all 21 models in our study. The Chinese mainland is divided into eight subregions based on administrative divisions and the characteristics of the monsoon climate over China (Shi and Xu 2007) (Fig. 1 and Table S2).

In our study, subregions 1 to 4 are in eastern China and subregions 5 to 8 are in western China.

2.2.1 Evaluation skill score

Two methods have been used to evaluate the performance of the NEX-GDDP data. First, for the spatial distribution of biases for TX and TN, we used the simulation value minus the observation value at each grid point. Second, Taylor diagrams (Taylor 2001) were used to evaluate the annual variation for TX and TN in the historical period. The Taylor diagram can succinctly summarize the relationship between model results and observations. Three statistics (the correlation coefficient, the root mean square error (RMSE) and the ratio of the standard deviations) are displayed in the diagram, which can more comprehensively and intuitively reflect the simulation ability of different models than any individual statistic.

2.2.2 Uncertainty analysis

The spatial distribution of changes in the trends for TX and TN in the future was calculated by evaluating values at each

grid point. To estimate the uncertainty for the average climate state over China in the future, we used an uncertainty analysis method described by Li and Zhou (2010). For measuring the effectiveness and reliability of the estimation results, we calculated a signal-to-noise ratio (SNR) as the ratio of the absolute value of variable variation (the anomaly value DN) to the standard deviation (SD). Here, DN took the absolute value of the difference between the MME value in the future period (2040–2069 and 2070–2099) and its baseline value (1970–1999) over China. The formulas for SD and SNR were as follows:

$$SD = \sqrt{\frac{1}{N} \sum_{i=0}^{i=N} (Y_i - \bar{Y})^2} \quad (1)$$

$$SNR = DN/SD \quad (2)$$

where N is the number of models, Y_i is the multi-year mean of the model i in the simulation period and \bar{Y} is the multi-year simulation mean of the MME.

3 Results

3.1 Evaluation of historical daily maximum and minimum temperatures

3.1.1 Spatial pattern

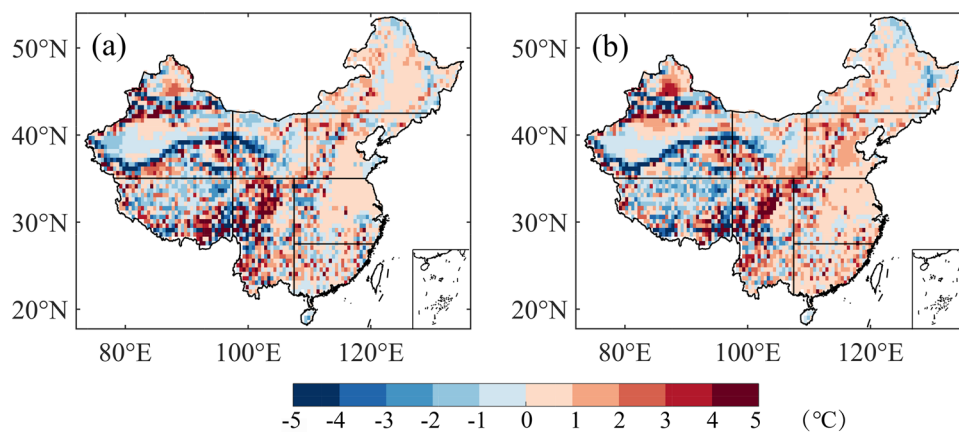
Figure 2 shows the spatial distribution of the biases in the simulation data (defined as the differences between the simulation and observation values) for TX and TN, respectively. We found that NEX-GDDP can capture the basic spatial patterns of TX and TN well, and simulation biases are relatively small. For TX, the simulation biases are mainly contributed by western China, and the biases in the west (2.03 °C) are 2.33 times the size of those in the east (0.87 °C). For TN, the

spatial distribution of simulation biases is similar to those of TX, and the biases in the west (1.92 °C) are 2.21 times the size of those in the east (0.87 °C). Xu and Xu (2012) found that simulation biases are also larger for temperature in western China than other subregions, which is relatively consistent with our results. With respect to seasonal patterns, the simulation biases of TX and TN are relatively small in winter (December–January–February (DJF)) and somewhat larger in summer (June–July–August (JJA)) (Fig. S1). But the difference in simulation biases between winter and summer is very small. For TX, the simulation biases are mainly contributed by summer, and the simulation biases in summer (1.74 °C) are 1.29 times the size of those in winter (1.35 °C). The simulation biases of TN and TX are similar, and the TN simulation biases in summer (1.53 °C) are 1.06 times the size of those in winter (1.45 °C).

Compared with the observations, simulation values for both TX and TN are overestimated over China, and the degree of overestimation is larger in the east than in the west. For TX, overestimation is mainly contributed by eastern China, and the contribution value in the east (0.33 °C) is 2.06 times the size of that in the west (0.16 °C). There are some similar results for TN. A previous study shows that the CMIP3/CMIP5 models tend to overestimate the temperature in northeastern China (Hua et al. 2014). Therefore, we can assume that the simulated overestimation in eastern China is mainly contributed by the overestimation in northeastern China. However, the degree of overestimation for TN is much larger than for TX, and the contribution value in the east (0.51 °C) is 5.67 times the size of the value in the west (0.09 °C). For winter and summer, both TX and TN are overestimated over China. Moreover, the difference between winter and summer is small, and it has been confirmed that the models in CMIP5 underestimate the differences between winter and summer rates of temperature rise (Liu et al. 2014).

We also found that MME simulation performs better than a single model. This conclusion has also been reached by

Fig. 2 Biases (simulation minus observation) for daily maximum temperature (a) and daily minimum temperature (b) of the MME over China from 1961 to 2005



previous researchers (Weisheimer et al. 2009). When compared with the observations, the simulation results still have some biases. On the whole, the subregion with the largest simulation biases for TX and TN is the Tibetan plateau (TP) (see Fig. 1 for subregion designations). The TP subregion contributed a large simulation error to western China. It may be that the thermal state of the ground is significantly affected by the terrain, and the large thermal differences and strong non-uniformity near the steep terrain lead to a large simulation bias. At the same time, we also found that the TP subregion temperatures were always underestimated in winter and summer. Previous research also revealed that the majority of the models in CMIP5 have cold biases over the Tibetan plateau (Su et al. 2012). The subregion with the smallest simulation biases for TX and TN is the middle of the WNW subregion (Tarim basin). The Taklamakan Desert, located in the center of the Tarim basin in southern Xinjiang, is the largest desert in China. The small size of the simulation biases there may be due to the fact that the desert terrain is flat and less affected by human activities than other areas. The simulation biases for TX and TN are also small in the Sichuan basin, which has been mentioned in previous studies (Bao and Wen 2017). Therefore, when studying these areas, we recommend the use of the NEX-GDDP dataset to obtain more accurate and reliable results. In addition,

the biases in NEX-GDDP may be caused by biases in the observations themselves that are used in the bias correction (Raghavan et al. 2018). Among the reasons for this, first consider that the eastern coastal subregion of China has been experiencing rapid urbanization (Li et al. 2015). Most of the meteorological observation stations in eastern China are no longer located in the original natural ecological environment. The meteorological observation stations in urban areas are now more affected by human activities than those in nonurban areas. To a large extent, this has led to distinct differences between the observational data from the eastern China meteorological observation stations and our actual, true meteorological values. Second, consider that the geographical conditions of western China are complex and diverse (Cheng et al. 2018). Using a small number of observation stations to represent the climate conditions of the entire vast western subregion will cause definite errors.

3.1.2 Temporal variation

The annual variation of TX (Fig. 3) and TN (Fig. 4) anomalies over China and different subregions is shown. In general, TX and TN fluctuate and rise yearly for observations and the MME, and the annual variation of TX is in good agreement with that of TN. According to TX and TN anomaly

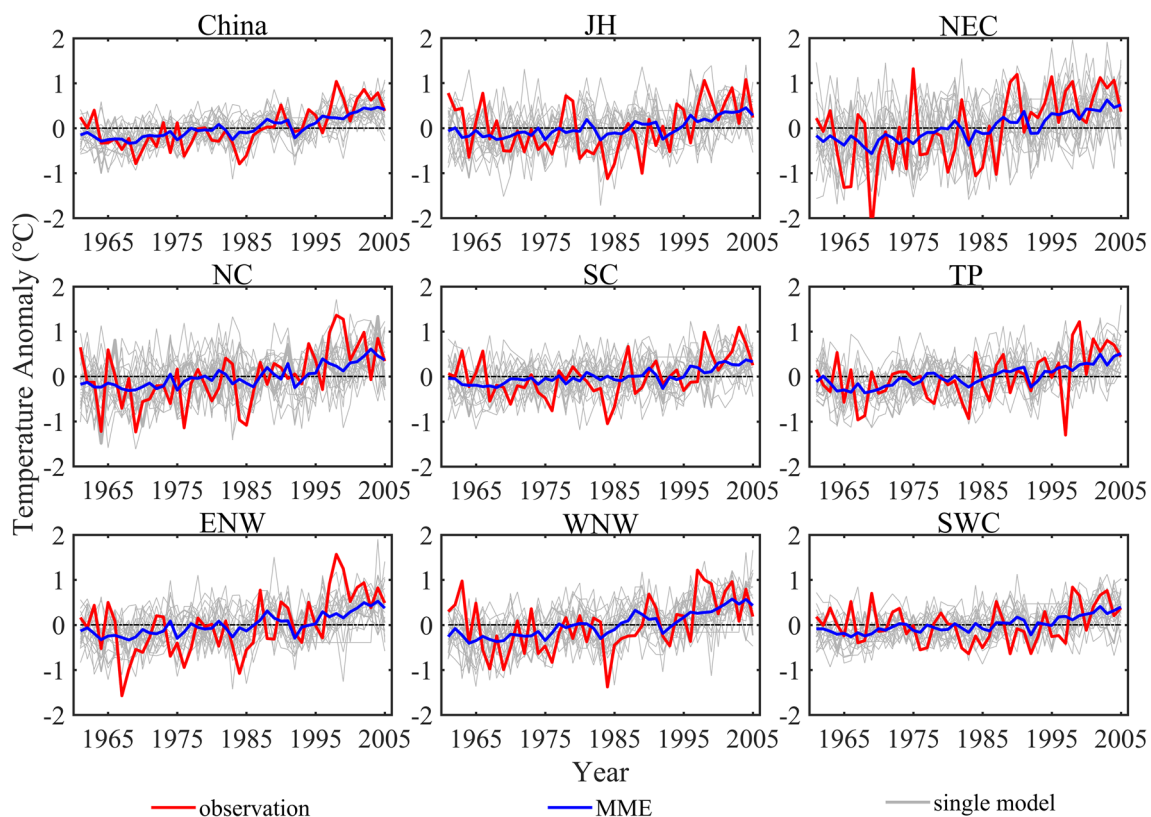


Fig. 3 Annual variation of daily maximum temperature anomalies over China and different subregions from 1961 to 2005

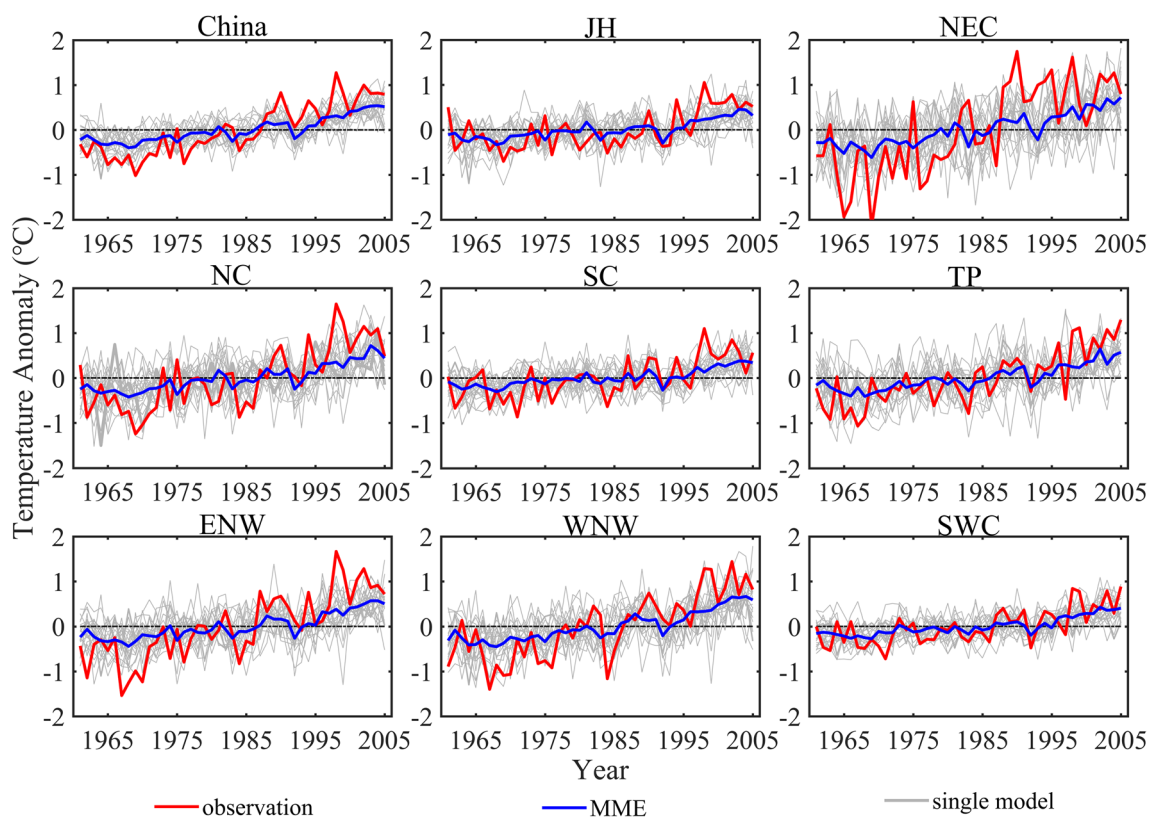


Fig. 4 Annual variation of daily minimum temperature anomalies over China and different subregions from 1961 to 2005

values for observations and the MME, the historical period can be divided into two periods: the anomaly values were mainly negative before 1985 and mainly positive after 1985. The warming trend of TX and TN accelerated notably after 1995. Compared with a single model, the MME can better simulate the overall trend of TX and TN change. However, compared with the observations, the MME still has some biases in simulating the annual variation of TX and TN, and the biases of TX are larger than those of TN. We also found that the TX and TN anomaly values of the MME are significantly less than those of the observations. In most subregions of China, the warming trends of the observations for TX and TN are greater than those of the MME. For TX, NEX-GDDP underestimated the warming trend over China, and the warming trend of the observations ($2.04\text{ }^{\circ}\text{C}/100\text{ yr}$) is 1.36 times that of the MME ($1.50\text{ }^{\circ}\text{C}/100\text{ yr}$). For TN, observations indicate an increase during the historical period of about $3.77\text{ }^{\circ}\text{C}/100\text{ yr}$, while the MME shows a relatively mild increase of about $1.81\text{ }^{\circ}\text{C}/100\text{ yr}$. Xu and Xu (2012) revealed that most CMIP5 models underestimated the actual temperature, which is consistent with our findings. For TX and TN, the subregion with the fastest warming trend over the past few decades for both observations and the MME is the NEC subregion. Previous studies have shown that the warming trend apparent across most of China was highest in

the northeast from 1955 to 2000 (Liu et al. 2004). The warming trend in the NEC subregion was underestimated, and the warming trend of TX for the observations ($3.27\text{ }^{\circ}\text{C}/100\text{ yr}$) is 1.69 times that of the MME ($1.94\text{ }^{\circ}\text{C}/100\text{ yr}$), while the warming trend of TN for the observations ($5.60\text{ }^{\circ}\text{C}/100\text{ yr}$) is 2.43 times that of the MME ($2.30\text{ }^{\circ}\text{C}/100\text{ yr}$). At the same time, we also found that the MME has the largest simulation biases for the NEC subregion. The warming trend is smallest for the observations in the SWC subregion, and smallest for the MME in the SC subregion. The poor simulation of warming trends over the past few decades may be due in part to the short time series of the historical periods. Past studies have found that climate models are better at simulating long-term climate sequences (Randall et al. 2007). In addition, the limited simulation capability of the climate model itself determines that the model simulation results deviate from observations (Flato et al. 2013).

To quantitatively evaluate the performance of NEX-GDDP for annual variation, the Taylor diagrams show three statistics to reflect the simulation ability of the different models (Fig. 5). The figures show the 21 NEX-GDDP models used in our study and their ensemble average compared with the observations on an annual scale. The lefthand diagram shows high correlation coefficients of models and observations, ranging from 0.4 to 0.7. Only values for the

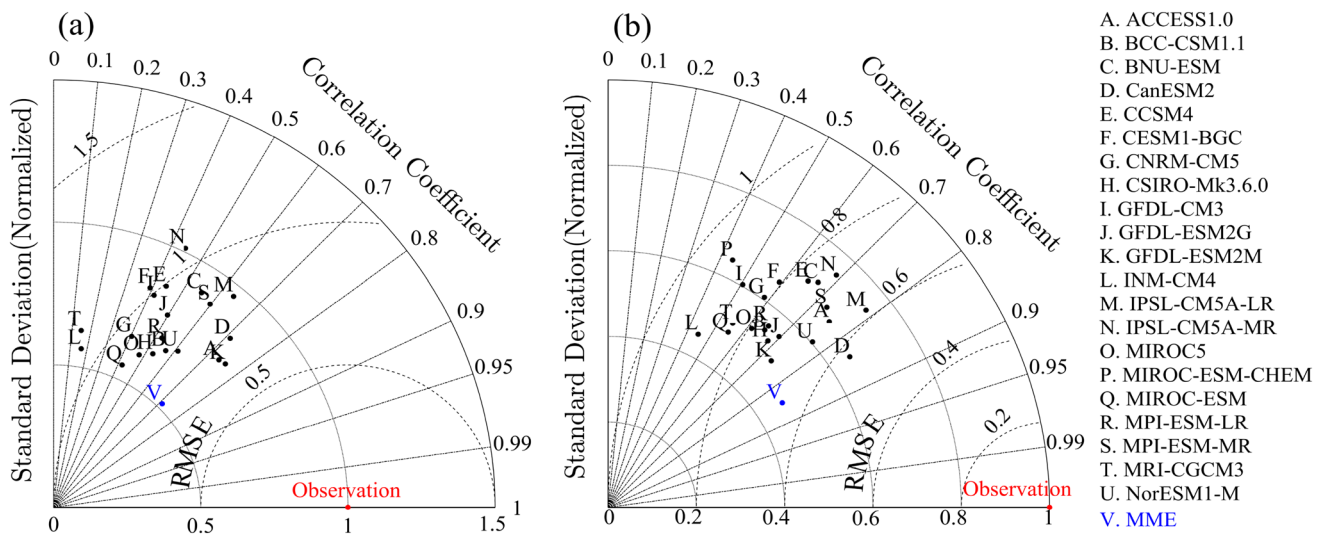


Fig. 5 Taylor diagrams for annual variation of daily maximum temperature (a) and daily minimum temperature (b) of observations and NEX-GDDP model data over China from 1961 to 2005

MME, ACCESS1.0, CanESM2 and GFDL-ESM2M are higher than 0.7, while those of INM-CM4 and MRI-CGCM3 are lower than 0.2. The RMSEs of the MME, ACCESS1.0, CanESM2 and GFDL-ESM2M are less than 0.8, while the RMSEs of INM-CM4, IPSL-CM5A-MR and MRI-CGCM3 are greater than 1. The ratios of standard deviations of most models are mainly between 0.5 and 1, and that of the MME is the least, close to 0.5. Compared with other models, the MME, ACCESS1.0, CanESM2 and GFDL-ESM2M have better simulation performance for the annual variation of TX over China. The righthand diagram shows high correlation coefficients between models and observations, ranging from 0.5 to 0.8. Those of the MME and CanESM2 are higher than 0.8, while those of INM-CM4 and MIROC-ESM-CHEM are lower than 0.5. The RMSEs of the MME, CanESM2 and IPSL-CM5A-LR are less than 0.65, while the RMSE of MIROC-ESM-CHEM is greater than 0.9. The ratios of standard deviations of all models are between 0.4 and 0.8, among which that of the MME is the smallest. Compared with other models, the MME, CanESM2 and IPSL-CM5A-LR have better simulation performance for the annual variation of TN over China. In general, the MME and CanESM2 are in better agreement with observations for the annual variation of TX and TN over China.

The monthly variation of TX (Fig. S2) and TN (Fig. S3) anomalies over China and its different subregions is shown in the supplemental information. In general, the monthly variation of TX is in good agreement with that of TN. For TX and TN, the observation temperature anomaly curves are in good agreement with the model temperature anomaly curves, which indicates that NEX-GDDP data is good at simulating the monthly variation of TX and TN in different

subregions. However, compared with the observations, there are some small simulation biases over China as a whole. TX and TN are underestimated slightly from January to February and overestimated slightly from June to September over China, but the biases are within 1 °C. In general, the MME has better simulation results for TX and TN in monthly variation than annual variation.

3.2 Projection of future changes in daily maximum and minimum temperatures

3.2.1 Spatial pattern of changes

For TX and TN, the warming is faster under the RCP8.5 scenario relative to the baseline, and the warming in the long-term is faster than that in the middle-term, which indicates that both TX and TN in the 21st century show a continuous rising trend (Fig. 6). The projected rates of rise of TX and TN in the 21st century are relatively similar. Under the RCP4.5 scenario, the warming relative to the baseline in the long-term is 1.26 (TX) and 1.24 (TN) times that in the middle-term over China; while under the RCP8.5 scenario, the warming relative to the baseline in the long-term is 1.66 (TX) and 1.65 (TN) times as much as that in the middle-term over China. Furthermore, the warming of the east is slower than that of the west in the future, but the contribution values to warming are not very different between the east and the west. This indicates that the warming over various subregions of China has a similar amplitude of variation in the 21st century.

Spatial patterns of changes relative to baseline in TX (Figs. S4–S7) and TN (Figs. S8–S11) for a single model

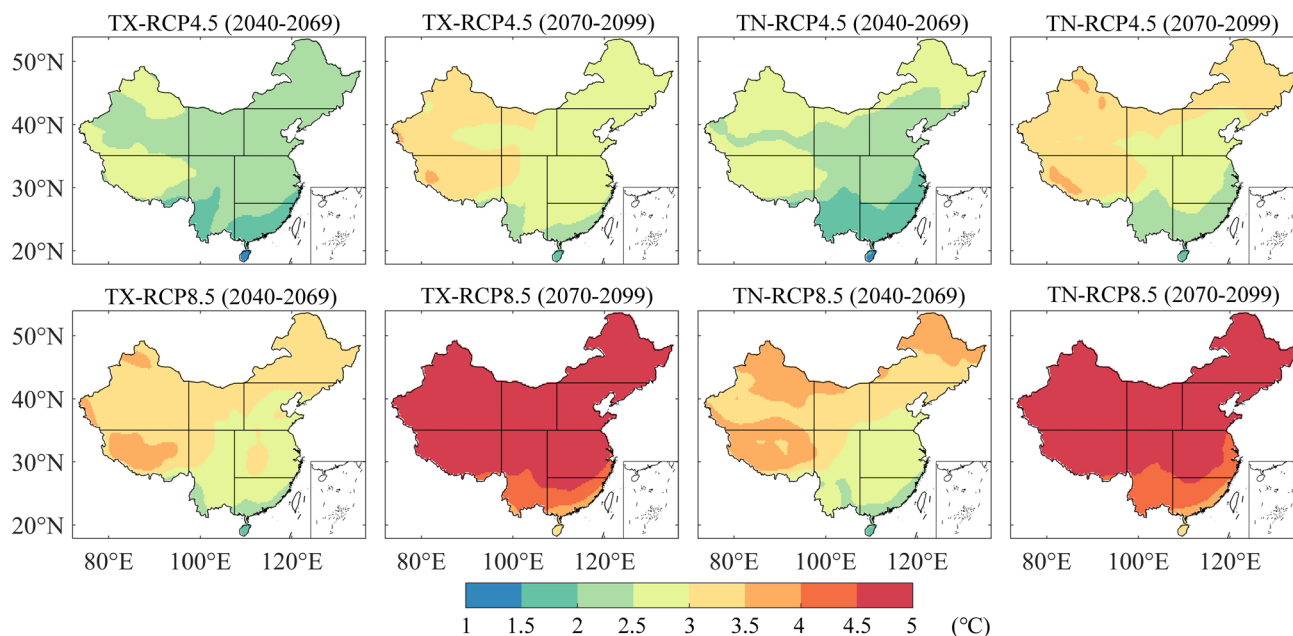


Fig. 6 Spatial patterns of changes in daily maximum and minimum temperatures in the middle-term (2040–2069) and long-term (2070–2099) relative to the baseline period (1970–1999) over China

over China in the future are quite different. Most models show that the changes in TX and TN are greater than 2 °C; CNRM-CM5, GFDL-ESM2G, GFDL-ESM2M, INM-CM4 and MRI-CGCM3 show slower warming, while GFDL-CM3, MIROC-ESM and MIROC-ESM-CHEM show faster warming, especially in the western subregions and the NEC subregion, which show more obvious warming than other subregions. The changes in TX and TN for most models under the RCP8.5 in the long-term are greater than 5 °C, which would have a great impact on the natural environment and human development by the end of the century.

Spatial patterns of changes for TX in winter and summer in the middle-term and long-term relative to the baseline are shown (Fig. 7). Under the RCP4.5 scenario, the warming of TX in the west is 1.11 (middle-term) and 1.09 (long-term) times as much as that in the east. Under the RCP8.5 scenario, the warming of TX in the west is 1.08 (middle-term) and 1.09 (long-term) times as much as that in the east. We found that the warming performance of TN is very similar to that of TX. This indicates that the warming changes of TX and TN are similar over different subregions of China, and the difference in warming between the west and the east is small. The warming of TX and TN fastest in the TP subregion in winter and fastest in the WNW subregion in summer, which results in more overall warming in the west than in the east.

By comparing the warming in winter and summer, we found that the warming of TX in winter is 1.05 (middle-term) and 1.07 (long-term) times as much as that in summer

under the RCP4.5 scenario, and the warming of TX in winter is 1.14 (middle-term) and 1.06 (long-term) times as much as that in summer under the RCP8.5 scenario. The warming performance of TN is very similar to that of TX in both winter and summer. The warming changes of TX and TN in winter are slightly higher than those in summer, and the difference is very small. Some studies have also shown that winter temperatures are increasing at a higher rate than summer temperatures (Liu et al. 2014) and that the inland areas in the northwest will warm much faster than areas in the southeast (Wang and Chen 2014). Other research suggests that winter warming will reach 5–6 °C over China in the long term (Bao and Wen 2017), which is consistent with our study results.

3.2.2 Uncertainty analysis

According to spatial patterns of standard deviation for TX and TN under the two scenarios (Fig. 8), the subregions with larger standard deviations are distributed mainly in western China, especially the TP and WNW subregions. In addition, the NEC subregion also shows larger standard deviations for TX and TN. This indicates that the uncertainties of TX and TN are relatively large in the above subregions. On the other hand, the uncertainties in the JH, SC and SWC subregions are relatively small, and spatial patterns of the signal-to-noise ratio (SNR) also show that it is higher in these areas with smaller uncertainties (Fig. 9). However, the uncertainties vary weakly between

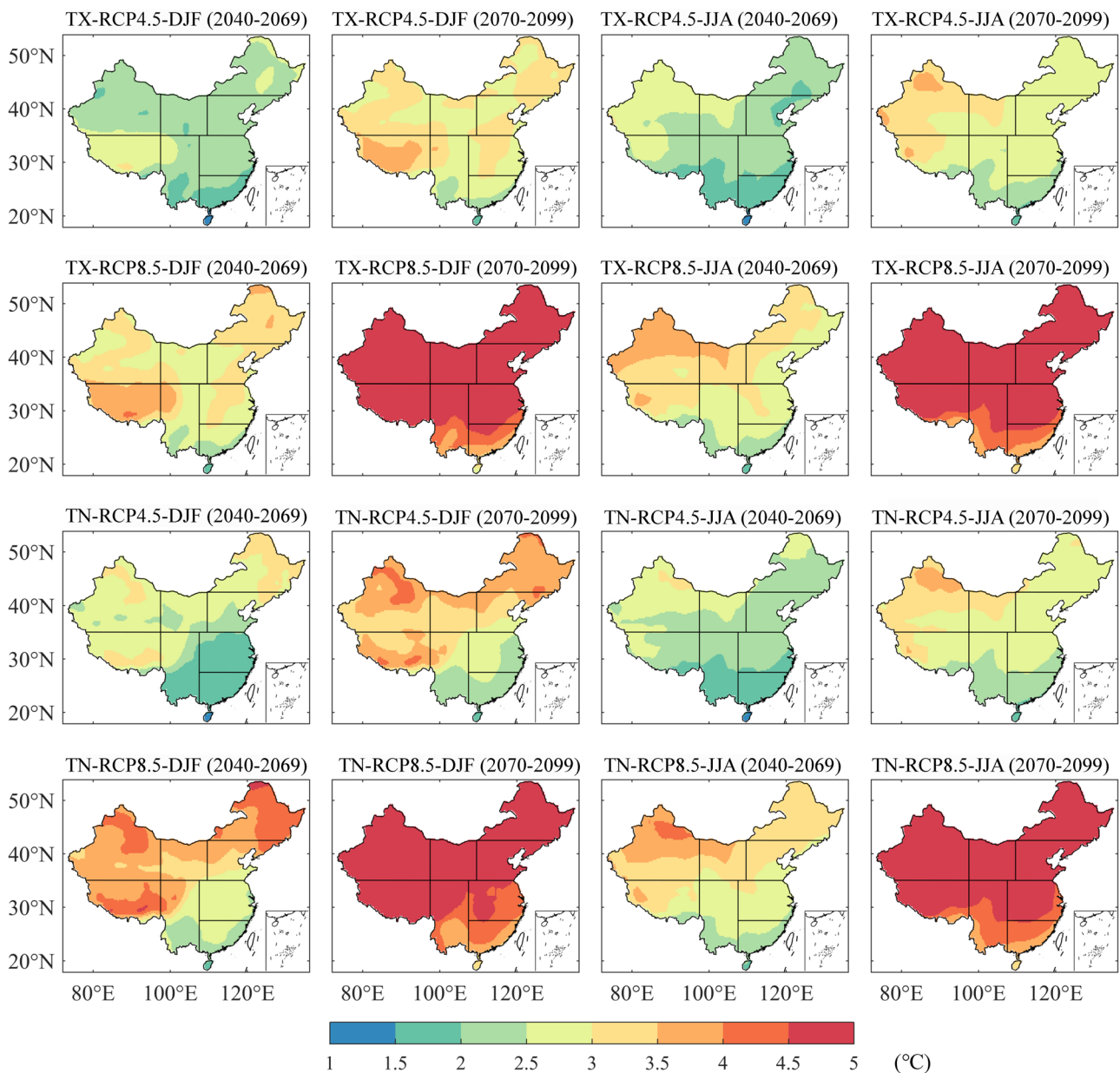


Fig. 7 Spatial patterns of changes for daily maximum and minimum temperatures in winter and summer in the middle-term (2040–2069) and long-term (2070–2099) relative to the baseline period (1970–1999) over China

the east and the west. As for specific performance, we found that under the RCP4.5 the uncertainties of TX in the west (0.73 °C for middle-term and 0.88 °C for long-term) are 1.1 times those in the east (0.64 °C for middle-term and 0.79 °C for long-term); and under the RCP8.5 the uncertainties of TX in the west (0.85 °C for middle-term and 1.26 °C for long-term) are 1.1 times those in the east (0.79 °C for middle-term and 1.12 °C for long-term). For TN, the spatial patterns of uncertainties are similar to

those of TX, and the differences between the east and the west are also very small.

The uncertainties over China under the RCP8.5 are greater than under the RCP4.5. For example, the uncertainties in the middle-term under the RCP8.5 (0.82 °C (TX) and 0.78 °C (TN)) are 1.3 times those under the RCP4.5 (0.65 °C (TX) and 0.62 °C (TN)), and the uncertainties in the long-term under the RCP8.5 (1.25 °C (TX) and 1.19 °C (TN)) are 1.5 times those under the RCP4.5 (0.85 °C (TX)

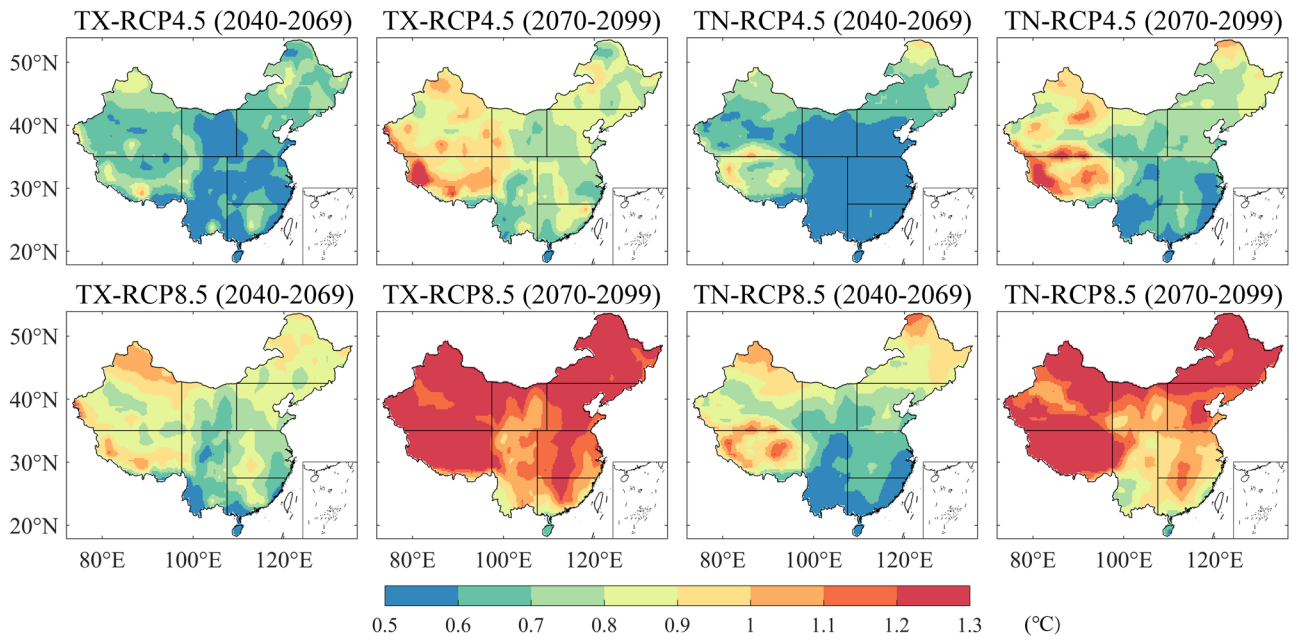


Fig. 8 Spatial patterns of standard deviation (SD) for daily maximum and minimum temperatures in the middle-term (2040–2069) and long-term (2070–2099) over China

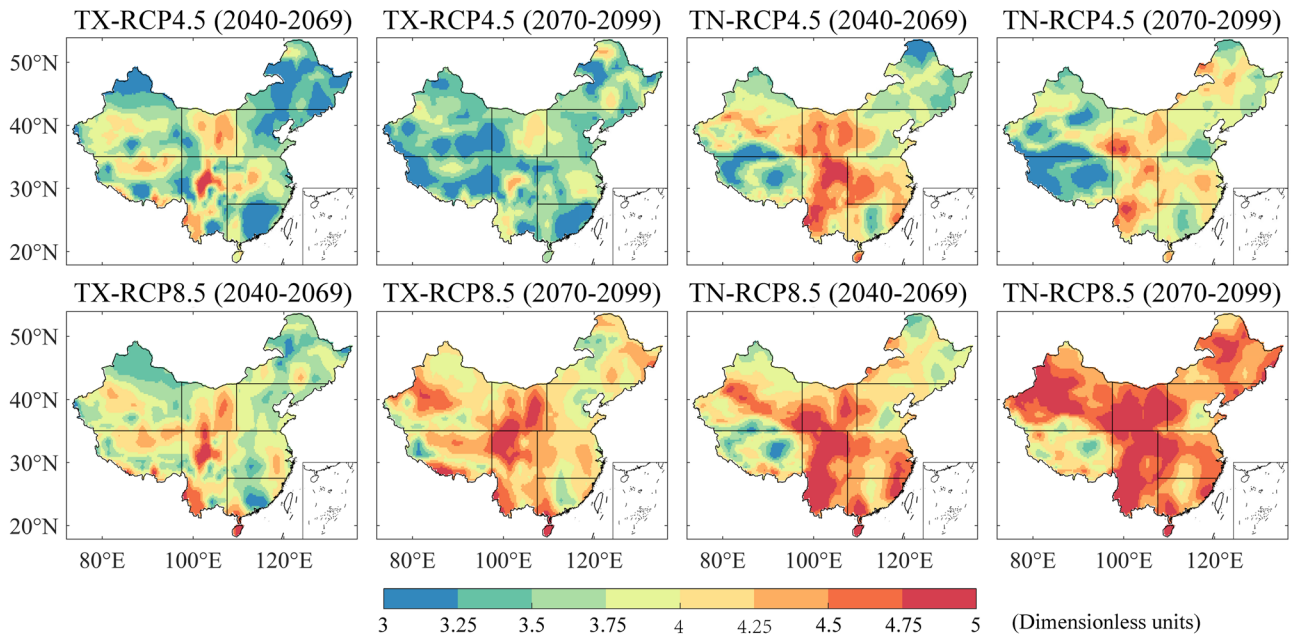


Fig. 9 Spatial patterns of the signal-to-noise ratio (SNR) for daily maximum and minimum temperatures in the middle-term (2040–2069) and long-term (2070–2099) over China

and 0.79 °C (TN)). We also found that the uncertainties over China in the long-term are greater than those in the middle-term. More specifically, the uncertainties under the RCP4.5 in the long-term are 1.3 times those in the middle-term, and the uncertainties under the RCP8.5 in the long-term are 1.5

times those in the middle-term. Previous studies have shown that higher warming changes correspond to greater uncertainties under the future scenarios (Meinshausen et al. 2011). For TX and TN, the signal-to-noise ratios of the simulation results over all subregions of China under the two scenarios

are greater than 1 (Fig. 9), which indicates that the output signals are larger than the noise values, and the reliabilities of the simulation results are higher than the uncertainties

caused by the simulation biases. The signal-to-noise ratios of the estimation results under the RCP8.5 are greater than those under the RCP4.5.

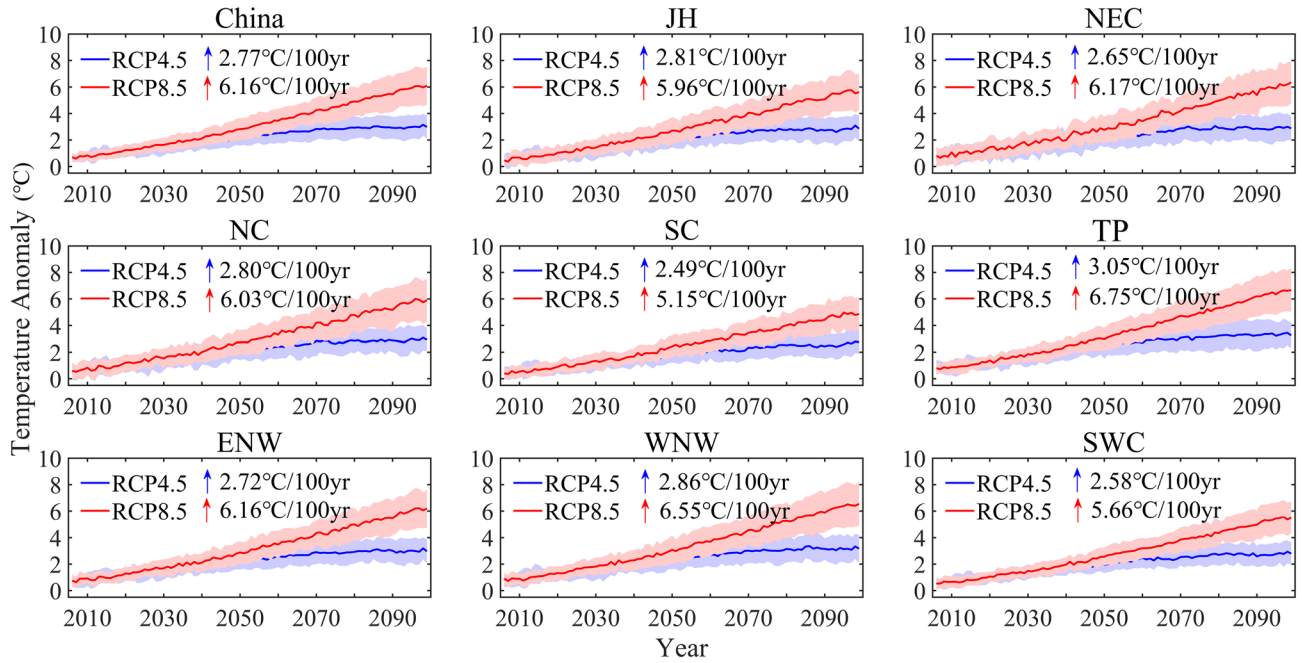


Fig. 10 Warming trends of daily maximum temperature over China and various subregions from 2006 to 2099. The values to the right of the blue arrows represent the warming trends under the RCP4.5

scenario, and the values to the right of the red arrows represent the warming trends under the RCP8.5 scenario

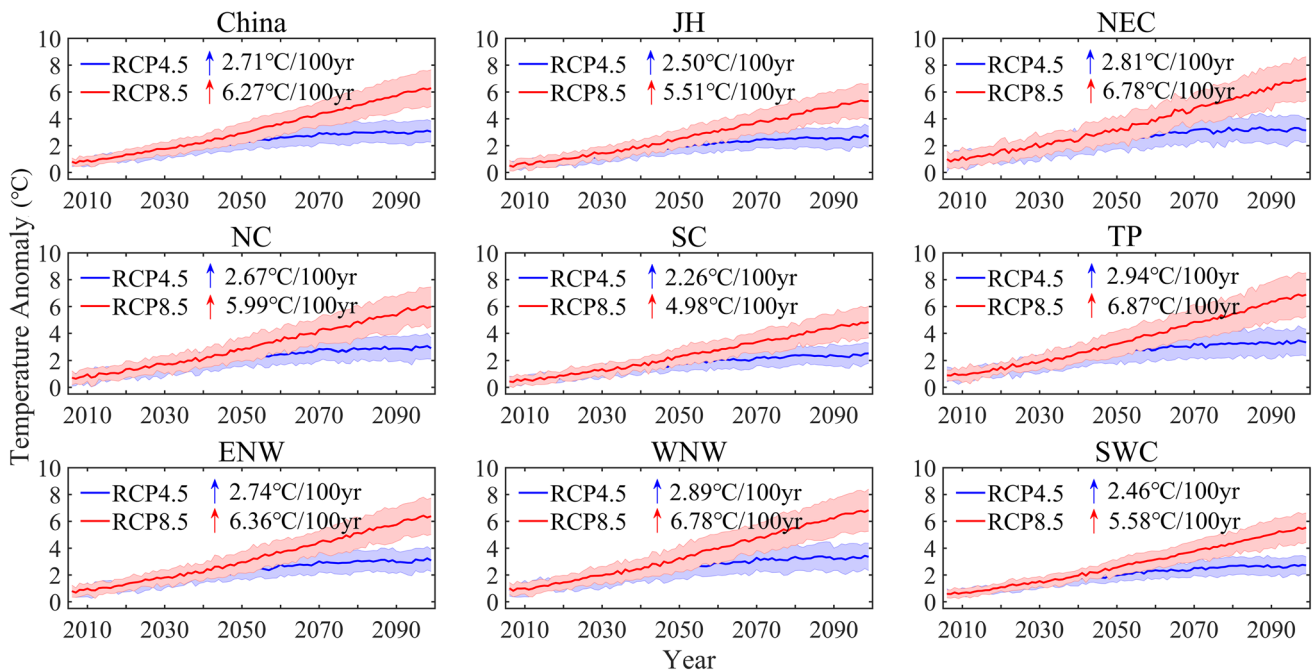


Fig. 11 Warming trends of daily minimum temperature over China and various subregions from 2006 to 2099. The values to the right of the blue arrows represent the warming trends under the RCP4.5

scenario, and the values to the right of the red arrows represent the warming trends under the RCP8.5 scenario

3.2.3 Regional temporal change

The annual variation trends of TX (Fig. 10) and TN (Fig. 11) over China and different subregions are shown. The blue (RCP4.5) and red (RCP8.5) lines represent annual variation trends of TX and TN under the two future scenarios. The shadings in light red and blue represent one standard deviation of TX and TN, as the range of uncertainties from the 21 models in NEX-GDDP. In the future, TX and TN over China and all subregions will continue to rise, and the warming trends will accelerate significantly under the RCP8.5. By the end of the century, TX and TN over China have a similar rising range. The increasing trend of TX under the RCP8.5 ($6.16\text{ }^{\circ}\text{C}/100\text{ yr}$) is 2.22 times that under the RCP4.5 ($2.77\text{ }^{\circ}\text{C}/100\text{ yr}$), and the increasing trend of TN under the RCP8.5 ($6.27\text{ }^{\circ}\text{C}/100\text{ yr}$) is 2.31 times that under the RCP4.5 ($2.71\text{ }^{\circ}\text{C}/100\text{ yr}$). This is very close to the results of previous studies in CMIP5 that estimated a warming trend from 2011 to 2100 of $0.24\text{ }^{\circ}\text{C}/10\text{ yr}$ for RCP4.5 and $0.63\text{ }^{\circ}\text{C}/10\text{ yr}$ for RCP8.5 (Xu and Xu 2012).

Under the RCP4.5, the subregion with the fastest warming trends is the TP subregion ($3.05\text{ }^{\circ}\text{C}/100\text{ yr}$ (TX) and $2.94\text{ }^{\circ}\text{C}/100\text{ yr}$ (TN)), while the SC subregion has the slowest warming trends ($2.49\text{ }^{\circ}\text{C}/100\text{ yr}$ (TX) and $2.26\text{ }^{\circ}\text{C}/100\text{ yr}$ (TN)). Under the RCP8.5, the warming trends of TX and TN in various subregions are similar to those under the RCP4.5. Moreover, we find that the difference of warming trends between the TP and SC subregions is increasing under the RCP8.5, which indicates that the warming of the TP subregion accelerates significantly under the RCP8.5. Based on what has been discussed above, under both RCP4.5 and RCP8.5 the TP subregion has the fastest warming trends. This may be due to the high altitude of the TP subregion itself and the low temperature base, making its warming trends the fastest among the eight subregions under global warming. As a southern region of China, the SC subregion has a low latitude and a high temperature base, so its warming trends are not as obvious as those in the TP subregion.

Both the red and blue shaded areas expand year by year, which indicates that the uncertainties of the simulation results also increase over time under the two scenarios. Moreover, the ranges of uncertainties under the RCP8.5 are larger than those under the RCP4.5, which is consistent with the uncertainty analysis results in Sect. 3.2.2. We think that the uncertainty ranges are not only related to the original CMIP5 model data (Taylor et al. 2012) but also affected by various downscaling methods (Woznicki et al. 2016).

4 Summary and conclusions

Evaluation and projection of daily maximum temperature (TX) and daily minimum temperature (TN) in the historical period (1961–2005) and the future period (2006–2099) over

China were performed using NEX-GDDP data. The results of the analysis show certain notable characteristics of NEX-GDDP in simulating TX and TN over China.

In general, NEX-GDDP can capture the basic spatial patterns of TX and TN, and multi-model ensemble (MME) simulation performs better than single-model simulations. When compared with the observations, the simulation results have some biases. The simulation biases of TX and TN are mainly contributed by western China, especially in summer, but the differences in simulation biases between winter and summer are very small. Among all subregions, the largest simulation biases are found in the TP subregion. Both TX and TN are overestimated over China relative to the observations, and the degree of overestimation in the east is much larger than that in the west. With respect to temporal scale, the MME has better simulation performance for TX and TN in monthly variation than annual variation. Our research found that NEX-GDDP data underestimated the warming trends of TX and TN from 1961 to 2005 over China. For TX and TN, the subregion with the largest warming trend over the past few decades is the NEC subregion, and it also has the largest simulation biases.

We also examined the warming changes over various subregions of China relative to the baseline period under two emissions scenarios. We found that the warming changes in TX and TN are similar over various subregions, and the differences in warming between the west and the east are small. The warming of TX and TN in the TP and WNW subregions is faster than that in other subregions. And the warming of TX and TN in winter is slightly higher than that in summer. We carried out an uncertainty analysis for TX and TN in the future periods (2040–2069 and 2070–2099). The results show that the differences in uncertainties are small between the east and the west. The uncertainties over China under the RCP8.5 are greater than those under the RCP4.5, and the uncertainties in the long-term are greater than those in the middle-term, which shows that higher warming changes correspond to greater uncertainties. We also found that the reliability of the simulation results is higher than the uncertainties caused by the simulation biases. To some extent, this indicates that NEX-GDDP is applicable for simulating TX and TN over China. By the end of the 21st century, the TP subregion has the fastest warming trend, while the warming of the SC subregion is relatively slow under the two scenarios. At the same time, the uncertainties of the simulation results are also increasing year by year.

We believe the high-resolution NEX-GDDP dataset will be widely used in the future, especially for regional climate change research when a high-resolution dataset is required. It not only provides long-time-scale information for the past and future, but also presents more detailed spatial scale information than the raw CMIP5 dataset. Our research results provide not only a reference significance

for data users but also a scientific basis for policy formulation in relevant governmental agencies and fields. At the same time, this study also has some shortcomings and limitations. Although China is divided into eight subregions in this paper, we focused mainly on comparison between the east and the west, so it is not clear whether there are significant differences between the simulation results of the north and the south. When evaluating the accuracy of TX and TN in the historical period, only one observational dataset was used, and the observational data itself may have some biases. Therefore, multi-source observational data should be used for further research. An ensemble of 21 models was used in our study, but if we remove some models with poor simulation performance and only retain those with good simulation ability, this would be beneficial for obtaining more accurate and reliable results, which will be carried out in our future work. In addition, users of NEX-GDDP data can try to use different multi-modal set averaging methods, which may produce additional useful conclusions. It is suggested that future data users consider the deficiencies and limitations we mentioned above to improve their work.

Acknowledgments This research was supported by the Second Tibetan Plateau Scientific Expedition and Research (2019QZKK0405), the National Natural Science Foundation of China (No. 41877155), and the National Key Research and Development Program of China (No. 2018YFC0507004). We are grateful to the China Meteorological Administration (CMA) for providing the observed climatic data (<http://data.cma.cn/>) and the NASA Ames Research Center for providing the NEX-GDDP dataset (<https://cds.nccs.nasa.gov/nex-gddp/>). We would like to thank the high-performance computing support from the Center for Geodata and Analysis, Faculty of Geographical Science, Beijing Normal University (<https://gda.bnu.edu.cn/>).

References

- Ahmadalipour A, Moradkhani H, Svoboda M (2017) Centennial drought outlook over the CONUS using NASA-NEX downscaled climate ensemble. *Int J Climatol* 37(5):2477–2491. <https://doi.org/10.1002/joc.4859>
- Ali J, Syed KH, Gabriel HF, Saeed F, Ahmad B, Bukhari SAA (2018) Centennial heat wave projections over Pakistan using ensemble NEX GDDP data set. *Earth Syst Environ* 2(3):437–454. <https://doi.org/10.1007/s41748-018-0064-8>
- Bao Y, Wen X (2017) Projection of China's near- and long-term climate in a new high-resolution daily downscaled dataset NEX-GDDP. *J Meteorol Res* 31(1):236–249. <https://doi.org/10.1007/s13351-017-6106-6>
- Blöschl G, Hall J, Parajka J, Perdigão RAP, Merz B, Arheimer B, Živković N (2017) Changing climate shifts timing of European floods. *Science* 357(6351):588. <https://doi.org/10.1126/science.aan2506>
- Cao F, Gao T (2019) Effect of climate change on the centennial drought over China using high-resolution NASA-NEX downscaled climate ensemble data. *Theor Appl Climatol* 138(1–2):1189–1202. <https://doi.org/10.1007/s00704-019-02895-9>
- Chen HP, Sun JQ, Li H-X (2017) Future changes in precipitation extremes over China using the NEX-GDDP high-resolution daily downscaled data-set. *Atmos Ocean Sci Lett* 10(6):403–410. <https://doi.org/10.1080/16742834.2017.1367625>
- Cheng Y, Liu H, Wang H, Hao Q (2018) Differentiated climate-driven Holocene biome migration in western and eastern China as mediated by topography. *Earth Sci Rev* 182:174–185. <https://doi.org/10.1016/j.earscirev.2018.05.006>
- Dale A, Fant C, Strzepek K, Lickley M, Solomon S (2017) Climate model uncertainty in impact assessments for agriculture: a multi-ensemble case study on maize in sub-Saharan Africa. *Earth's Future* 5(3):337–353. <https://doi.org/10.1002/2017ef000539>
- Dawson TP, Perryman AH, Osborne TM (2014) Modelling impacts of climate change on global food security. *Clim Change* 134(3):429–440. <https://doi.org/10.1007/s10584-014-1277-y>
- Flato G, Marotzke J, Abiodun B, Braconnot P, Chou SC, Collins W, Cox P, Driouech F, Emori S, Eyring V, Forest C, Gleckler P, Guilyardi E, Jakob C, Kattsov V, Reason C, Rummukainen M (2013) Evaluation of climate models. In: Stocker TF, Qin D, Plattner GK, Tignor M, Allen SK, Boschung J, Nauels A, Xia Y, Bex V, Midgley PM (eds) *Climate change 2013: The physical science basis. Contribution of working group I to the fifth assessment report of the intergovernmental panel on climate change*. Cambridge University Press, Cambridge
- Gao X, Shi Y, Zhang D, Giorgi F (2012) Climate change in China in the 21st century as simulated by a high resolution regional climate model. *Chin Sci Bull* 57(10):1188–1195. <https://doi.org/10.1007/s11434-011-4935-8>
- Gosling SN, Arnell NW (2013) A global assessment of the impact of climate change on water scarcity. *Clim Change* 134(3):371–385. <https://doi.org/10.1007/s10584-013-0853-x>
- Gou J, Miao C, Duan Q, Tang Q, Di Z, Liao W, Wu J, Zhou R (2020) Sensitivity analysis-based automatic parameter calibration of the VIC model for streamflow simulations over China. *Water Resources Res* 56(1):e2019WR025968. <https://doi.org/10.1029/2019WR025968>
- Guo D, Wang H (2016) Comparison of a very-fine-resolution GCM with RCM dynamical downscaling in simulating climate in China. *Adv Atmos Sci* 33(5):559–570. <https://doi.org/10.1007/s00376-015-5147-y>
- Hua W, Chen H, Sun S (2014) Uncertainty in land surface temperature simulation over China by CMIP3/CMIP5 models. *Theor Appl Climatol* 117:463–474. <https://doi.org/10.1007/s00704-013-1020-z>
- Huang D, Zhang L, Gao G, Sun S (2018) Projected changes in population exposure to extreme heat in China under a RCP8.5 scenario. *J Geogr Sci* 28(10):1371–1384. <https://doi.org/10.1007/s11442-018-1550-5>
- IPCC (2014) In: Field CB, Barros VR, Dokken DJ, Mach KJ, Mastrandrea MD, Bilir TE, Chatterjee M, Ebi KL, Estrada YO, Genova RC, Girma B, Kissel ES, Levy AN, MacCracken S, Mastrandrea PR, White LL (eds) *Climate change 2014: impacts, adaptation, and vulnerability. part a: global and sectoral aspects. contribution of working group II to the fifth assessment report of the intergovernmental panel on climate change*. Cambridge University Press, Cambridge
- Jain S, Salunke P, Mishra SK, Sahany S, Choudhary N (2019) Advantage of NEX-GDDP over CMIP5 and CORDEX data: Indian summer monsoon. *Atmos Res* 228:152–160. <https://doi.org/10.1016/j.atmosres.2019.05.026>
- Jiang D, Tian Z, Lang X (2016) Reliability of climate models for China through the IPCC third to fifth assessment reports. *Int J Climatol* 36(3):1114–1133. <https://doi.org/10.1002/joc.4406>
- Li B, Zhou TJ (2010) Projected climate change over China under SRES AIB scenario: Multi-model ensemble and uncertainties. *Adv Clim Change Res* 6(4):270–276
- Li J, Deng J, Gu Q, Wang K, Ye F, Xu Z, Jin S (2015) The accelerated urbanization process: a threat to soil resources in Eastern China. *Sustainability* 7:7137–7155. <https://doi.org/10.3390/su7067137>

- Liu B, Xu M, Henderson M, Qi Y, Li Y (2004) Taking China's temperature: daily range, warming trends, and regional variations, 1955–2000. *J Clim* 17(22):4453–4462. <https://doi.org/10.1175/3230.1>
- Liu S, Gao W, Liang XZ (2012) A regional climate model downscaling projection of China future climate change. *Clim Dyn* 41(7–8):1871–1884. <https://doi.org/10.1007/s00382-012-1632-5>
- Liu Y, Feng J, Ma Z (2014) An analysis of historical and future temperature fluctuations over China based on CMIP5 simulations. *Adv Atmos Sci* 31(2):457–467. <https://doi.org/10.1007/s00376-013-3093-0>
- Matthews TK, Wilby RL, Murphy C (2017) Communicating the deadly consequences of global warming for human heat stress. *Proc Natl Acad Sci USA* 114(15):3861–3866. <https://doi.org/10.1073/pnas.1617526114>
- Maurer EP, Hidalgo HG (2008) Utility of daily vs. monthly large-scale climate data: an intercomparison of two statistical downscaling methods. *Hydrol Earth Syst Sci* 12(2):551–563. <https://doi.org/10.5194/hess-12-551-2008>
- Mazdiyasi O, AghaKouchak A (2015) Substantial increase in concurrent droughts and heatwaves in the United States. *Proc Natl Acad Sci USA* 112(37):11484–11489. <https://doi.org/10.1073/pnas.1422945112>
- Meinshausen M, Smith SJ, Calvin K, Daniel JS, Kainuma MLT, Lamarque JF, van Vuuren DPP (2011) The RCP greenhouse gas concentrations and their extensions from 1765 to 2300. *Clim Change* 109(1–2):213–241. <https://doi.org/10.1007/s10584-011-0156-z>
- Nauman S, Zulkafli Z, Bin Ghazali AH, Yusuf B (2019) Impact assessment of future climate change on streamflows upstream of Khanpur Dam, Pakistan using soil and water assessment tool. *Water*. <https://doi.org/10.3390/w11051090>
- Raghavan SV, Hur J, Liang SY (2018) Evaluations of NASA NEX-GDDP data over Southeast Asia: present and future climates. *Clim Change* 148(4):503–518. <https://doi.org/10.1007/s10584-018-2213-3>
- Randall DA, Wood RA, Bony S, Colman R, Fichetef T, Fyfe J, Kattsov V, Pitman A, Shukla J, Srinivasan J, Stouffer RJ, Sumi A, Taylor KE (2007) Climate Models and Their Evaluation. In: Solomon S, Qin D, Manning M, Chen Z, Marquis M, Averyt KB, Tignor M, Miller HL (eds) *Climate Change 2007: the physical science basis*. Contribution of working group I to the fourth assessment report of the intergovernmental panel on climate change. Cambridge University Press, Cambridge
- Semakula HM, Song G, Achuu SP, Shen M, Chen J, Mukwaya PI, Zhang S (2017) Prediction of future malaria hotspots under climate change in sub-Saharan Africa. *Clim Change* 143(3–4):415–428. <https://doi.org/10.1007/s10584-017-1996-y>
- Shi X, Xu X (2007) Regional characteristics of the interdecadal turning of winter/summer climate modes in Chinese mainland. *Chin Sci Bull* 52(1):101–112. <https://doi.org/10.1007/s11434-007-0007-5>
- Slater LJ, Villarini G, Bradley AA (2016) Evaluation of the skill of North-American Multi-Model Ensemble (NMME) global climate models in predicting average and extreme precipitation and temperature over the continental USA. *Clim Dyn* 53(12):7381–7396. <https://doi.org/10.1007/s00382-016-3286-1>
- Smith SJ, Edmonds J, Hartin CA, Mundra A, Calvin K (2015) Near-term acceleration in the rate of temperature change. *Nat Clim Change* 5(4):333–336. <https://doi.org/10.1038/nclimate2552>
- Su F, Duan X, Chen D, Hao Z, Cuo L (2012) Evaluation of the global climate models in the CMIP5 over the Tibetan Plateau. *J Clim* 26(10):3187–3208. <https://doi.org/10.1175/JCLI-D-12-00321.1>
- Sun Q, Miao C, Hanel M, Borthwick AGL, Duan Q, Ji D, Li H (2019) Global heat stress on health, wildfires, and agricultural crops under different levels of climate warming. *Environ Int* 128:125–136. <https://doi.org/10.1016/j.envint.2019.04.025>
- Sun Q, Miao C, AghaKouchak A, Mallakpour I, Ji D, Duan Q (2020) Possible increased frequency of ENSO-related dry and wet conditions over some major watersheds in a warming climate. *Bull Am Meteor Soc* 101(4):E409–E426
- Sunyer MA, Madsen H, Ang PH (2012) A comparison of different regional climate models and statistical downscaling methods for extreme rainfall estimation under climate change. *Atmos Res* 103:119–128. <https://doi.org/10.1016/j.atmosres.2011.06.011>
- Taylor KE (2001) Summarizing multiple aspects of model performance in a single diagram. *J Geophys Res* 106(D7):7183–7192. <https://doi.org/10.1029/2000jd900719>
- Taylor KE, Stouffer RJ, Meehl GA (2012) An overview of CMIP5 and the experiment design. *Bull Am Meteor Soc* 93(4):485–498. <https://doi.org/10.1175/bams-d-11-00094.1>
- Thilakarathne M, Sridhar V (2017) Characterization of future drought conditions in the lower Mekong River Basin. *Weather Clim Extrem* 17:47–58. <https://doi.org/10.1016/j.wace.2017.07.004>
- Thrasher B, Maurer EP, McKellar C, Duffy PB (2012) Technical Note: bias correcting climate model simulated daily temperature extremes with quantile mapping. *Hydrol Earth Syst Sci* 16(9):3309–3314. <https://doi.org/10.5194/hess-16-3309-2012>
- Thrasher B, Xiong J, Wang W, Melton F, Michaelis A, Nemani R (2013) Downscaled climate projections suitable for resource management. *Eos Trans Am Geophys Union* 94(37):321–323. <https://doi.org/10.1002/2013EO370002>
- Wang L, Chen W (2014) A CMIP5 multimodel projection of future temperature, precipitation, and climatological drought in China. *Int J Climatol* 34(6):2059–2078. <https://doi.org/10.1002/joc.3822>
- Weisheimer A, Doblas-Reyes FJ, Palmer TN, Alessandri A, Arribas A, Déqué M, Rogel P (2009) ENSEMBLES: A new multi-model ensemble for seasonal-to-annual predictions—Skill and progress beyond DEMETER in forecasting tropical Pacific SSTs. *Geophys Res Lett* 36(21):L08801. <https://doi.org/10.1029/2009gl040896>
- Wood, A. W., Maurer, E. P., Kumar, A., & Lettenmaier, D. P. (2002). Long-range experimental hydrologic forecasting for the eastern United States. *Journal of Geophysical Research: Atmospheres*, 107(D20), ACL 6-1-ACL 6-15. <https://doi.org/10.1029/2001JD000659>
- Wood AW, Leung LR, Sridhar V, Lettenmaier DP (2004) Hydrologic implications of dynamical and statistical approaches to downscaling climate model outputs. *Clim Change* 62(1):189–216. <https://doi.org/10.1023/B:CLIM.0000013685.99609.9e>
- Woznicki SA, Nejadhashemi AP, Tang Y, Wang L (2016) Large-scale climate change vulnerability assessment of stream health. *Ecol Ind* 69:578–594. <https://doi.org/10.1016/j.ecolind.2016.04.002>
- Xu C, Xu Y (2012) The projection of temperature and precipitation over China under RCP Scenarios using a CMIP5 multi-model ensemble. *Atmos Ocean Sci Lett* 5(6):527–533. <https://doi.org/10.1080/16742834.2012.11447042>
- Yin H, Donat MG, Alexander LV, Sun Y (2015) Multi-dataset comparison of gridded observed temperature and precipitation extremes over China. *Int J Climatol* 35(10):2809–2827. <https://doi.org/10.1002/joc.4174>
- Zhang L, Yang B, Li S, Hou Y, Huang D (2018a) Potential rice exposure to heat stress along the Yangtze River in China under RCP8.5 scenario. *Agric For Meteorol* 248:185–196. <https://doi.org/10.1016/j.agrformet.2017.09.020>
- Zhang Y, You Q, Mao G, Chen C, Ye Z (2018b) Short-term concurrent drought and heatwave frequency with 1.5 and 2.0 C global warming in humid subtropical basins: a case study in the Gan

- River Basin, China. *Clim Dyn* 52(7–8):4621–4641. <https://doi.org/10.1007/s00382-018-4398-6>
- Zheng H, Miao C, Wu J, Lei X, Liao W, Li H (2019) Temporal and spatial variations in water discharge and sediment load on the Loess Plateau, China: a high-density study. *Sci Total Environ* 666:875–886. <https://doi.org/10.1016/j.scitotenv.2019.02.246>
- Zhou T, Yu R (2006) Twentieth-Century surface air temperature over china and the globe simulated by coupled climate models. *J Clim* 19(22):5843–5858. <https://doi.org/10.1175/JCLI3952.1>
- Publisher's Note** Springer Nature remains neutral with regard to jurisdictional claims in published maps and institutional affiliations.